OPTIMISATION OF SELF-PUNCHING RIVETING PROCESS PARAMETERS FOR HIGH-SPEED RAIL TOP PLATES

Qingchun ZHENG[1,2], Chengmin GUO[1,2], Peihao ZHU[1,2,*], Jiaqi LIU[1,2], Wenpeng MA[1,2], Shuoshuo ZHAO[1,2]

To improve the quality of self-pierce riveted joints, this paper uses a multi-objective optimisation method that incorporates a quadratic polynomial response surface model and the NSGA-II algorithm to optimise the parameters of the self-pierce riveting process. First, we carry out finite element simulations of the self-pierce riveted joint to determine the main factors affecting the quality of the joint forming through sensitivity analysis, and specify the optimum range of each parameter. Second, we use central composite design experiments to establish a quadratic polynomial response surface model. Third, we optimise the multi-objective model by using the NSGA-II algorithm and obtain the Pareto optimal solution. Finally, we use cross-sectional measurement and mechanical properties experiments to verify the feasibility of optimising the self-pierce riveted joint. The experimental results show that the bottom thickness increases by 24.7%, the undercut amount by 14.5%, and the tensile shear force by 27% compared to the pre-optimisation period. The quality of the riveted joints was significantly improved after optimisation, laying a good foundation for improving the safety of high-speed railway bodies.

Keywords: self-pierce riveting, sensitivity analysis, central composite design experiments, response surface model, multi-objective optimisation

1. Introduction

In recent years, high-speed railway technology has developed rapidly, and the manufacturing requirements and environmental standards of the high-speed railway have been continuously improved. To further enhance its competitiveness, the field of high-speed railway manufacturing needs to make the structural lightweight of its products a top priority for future body manufacturing [1]. Self-pierce riveting is the primary connection method in manufacturing high-speed railway bodies. As aluminium alloy sheets of different elongation and thicknesses are used for each connection, this makes the force requirements for different riveting parts of the body differently and place higher demands on the parameters of the self-pierce riveting process.

[1] Tianjin Key Laboratory for Advanced Mechatronic System Design and Intelligent Control, School of Mechanical Engineering, Tianjin University of Technology, Tianjin 300384, China
[2] National Demonstration Center for Experimental Mechanical and Electrical Engineering Education (Tianjin University of Technology)
[*] Corresponding author: Peihao Zhu E-mail: 18953744027@163.com

To address this issue, a large number of studies have been conducted by scholars in various countries, and some research results have been obtained. Rezwanul [2] measured the performance of self-pierce riveted joints by cross-sectional dimensions and concluded that the joint quality is related to the rivet head height, bottom thickness, and other factors after analysis. Carandente et al. [3], to enhance the accuracy of the finite element numerical simulation, considered the role of frictional heat in the mechanical deformation process, and verified the accuracy of the finite element model by experiment. Xie et al. [4] used finite element numerical simulations and orthogonal tests to study the influence of tooling process parameters on the effect of dissimilar metal riveted joints and the key factors affecting their quality. Chung et al. [5] studied the tensile-shear properties of riveted joints in aluminium-steel material riveted joint fatigue strength of tensile and shear specimens, comparing the degree of influence of external load on the upper and lower plates. Zhang et al. [6] used genetic optimisation algorithms to optimise the rivet and die parameters, validated by finite element simulations. There is relatively little research on the integrated role of riveting process parameters when studying the self-pierce riveting process. Zhang considers multiple parameters, the combination obtained is not guaranteed to be globally optimal due to the limitations of the genetic optimisation algorithm and has not been validated experimentally. This paper addresses the drawbacks of the genetic algorithm by considering multiple riveting process parameters and using the NSGA-II algorithm for multi-objective optimisation. Finally, we use experiments to verify the effectiveness of this method.

2. Description and modeling of self-pierce riveting

2.1 Riveting process flow

The process flow of self-punch riveting is divided into the clamping, sprint, expansion, and riveting stages. First, fix the plate with the blank holder. Second, the rivet penetrates the upper plate under the action of the punch, the rivet nail leg is deformed in piercing the lower plate material. Finally, the riveting is completed. Fig. 1 shows the process [7].

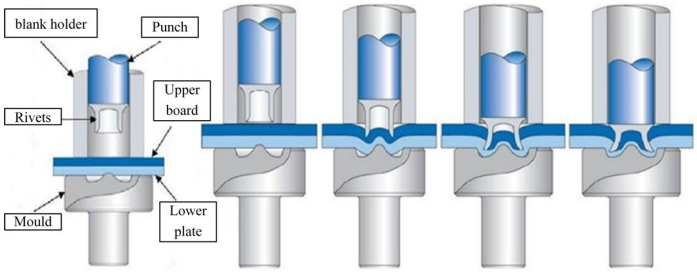

Fig 1 Riveting process flow.

2.2 Self-punching riveting process parameters

The main parameters affecting the quality of the self-pierce riveted head are the external processing parameters, such as punching load and speed, as well as the model parameters, such as rivet and die parameters [8]. Because rivet length will affect the amount of rivet flaring [9]; rivet diameter will affect the residual stress and top sealing [10]; the punching speed will affect the geometric shape of the joint and the penetration of the rivet [11]; die depth, die bottom radius and die radius will affect the joint and stability of rivet riveting [12]. So, this paper mainly focuses on parameters such as punching speed v, die depth h, rivet length L, rivet diameter d, die bottom radius r, and die radius R from a comprehensive perspective. Figure 2 shows the model parameters.

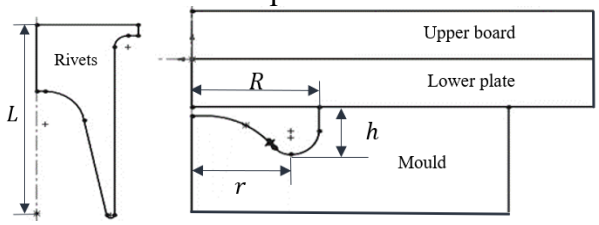

Fig 2 Self-piercing riveting process parameters.

2.3 Self-pierce riveted joint performance evaluation index

In this study, we consider the cross-sectional dimensions of the self-pierce riveted joint head as the top index to comprehensively evaluate the quality of the joint. In Figure 3, the main cross-sectional parameters for evaluating the forming quality of the joint are the height of the nailhead, bottom thickness, undercut amount, and rivet opening [13]. Among them, this paper mainly considers the bottom thickness S and the undercut amount D according to the actual demand.

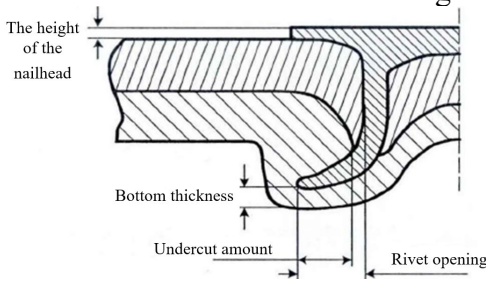

Fig 3 Connector section parameters.

2.4 Self-punch riveting finite element modeling and verification

First, we select a riveted part of the high-speed rail roof as the research object. Establish the model of the rivet, riveting plate, and die with the same structural dimensions in the display dynamics analysis module of ANSYS

Workbench. Table 1 shows the dimensions of each part. After taking the riveting part structure, actual working conditions and calculation time into account, select the riveting quarter model for FEA.

Table 1

Geometric dimensions of prototype riveted structure

	Rivet diameter	Rivet length	Die depth	Die radius	Die bottom radius	Plate thickness	Riveting plate length
Size	5.50mm	6.00mm	1.90mm	4.40mm	2.7mm	2.00mm	20mm

Then, the material of the riveting plate and rivet is 5083 aluminum alloy and MnB4, respectively. Set the die as a rigid body, and define the attributes of the riveting plate and rivet according to Table 2.

Table 2

Main parameters of riveting plate and rivet

	Density	Young's modulus	Poisson's Ratio	Yield Strength	Tangent Modulus
Al5083	2660kg/m²	7×10^4MPa	0.33	230MPa	315MPa
MnB_4	7850 kg/m²	1.5×10^5MPa	0.3	-	-

Then, we mesh the model. To reduce calculation time, the key position of the riveted plate is refined locally. Table 3 shows the number of grids for each part.

Table 3

Number of grids per part

	Upper board	Lower plate	Rivets	Die
Grid size	0.1mm	0.1mm	0.15mm	0.4mm
Number of grid	151952	151952	87584	56384

Then, we set the contact, including the contact between the upper and lower plate, the rivet and the plate, etc. Select the contact setting using Body Interactions. Then, set the die to fix. The aluminum alloy sheet does not move up and down except in the riveting area. The rivet only moves in the Z direction. The stamping speed is 10mm/s, and the total time is 0.8s. Finally, carry out dynamic FEA. The contact parameters are adjusted so that no breakage or ejection of the rivet foot section occurs after the formed joint. No mesh failure or distortion occurred in various parts. The process is shown in Fig. 4.

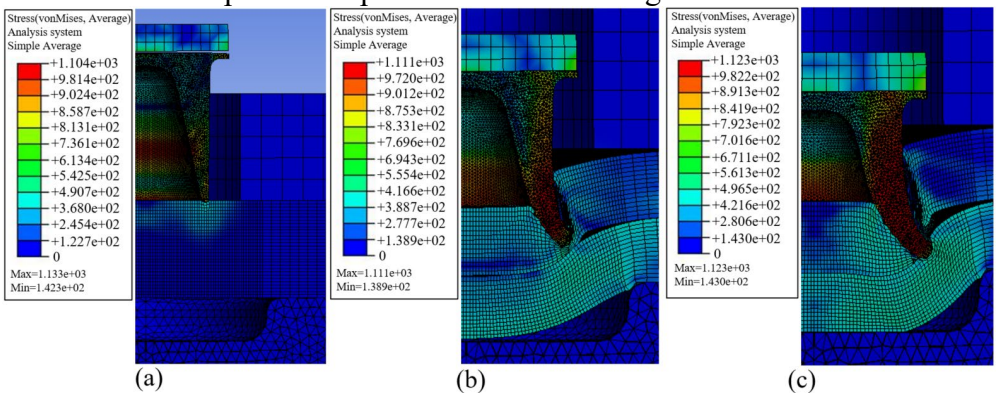

(a) (b) (c)

Fig 4 Self-thrust riveting simulation process.

To verify the realism of the finite element simulation, obtain cross-sectional dimensions of experimental joints by a two-dimensional digital image measurement instrument. Then, use HyperView to measure the simulated joint' cross-sectional dimensions. As seen in Table 4, all errors are within 10%, in line with the requirements of the engineering allowable error.

Table 4

Comparison of experimental and simulated values

	Bottom thickness	Undercut amount
Finite element simulation	0.97mm	0.71mm
Experiment	0.94mm	0.76mm
Error reduction rate	3.2%	6.6%

3. Analysis of riveting process parameters on a riveting performance

3.1 Sensitivity analysis of riveting process parameters

In this study, we perform sensitivity analysis [14] on six parameters such as punching speed v, die depth h, rivet length L, rivet diameter d, die bottom radius r and die radius R, extracting the parameter with the most significant influence on the joint performance. First, establish a riveting parameter analysis model, and define the sensitivity of mechanical properties to riveting parameters as the ratio of the relative increment of mechanical properties to riveting parameters caused by the increment of riveting parameters. The calculation process is shown in Equation (1).

$$SI_{ij} = \left| \frac{\Delta f_i}{\Delta \xi_j} \right| \tag{1}$$

In equation (1), $\Delta \xi_j$ denotes the relative increment of rivet parameters and $\Delta \xi_i = \frac{\Delta x_j}{x_j}$; Δf_i indicates the increment of mechanical properties.

For comparison purposes, we use equation (2) to normalize the sensitivity.

$$SI_{ij} = \frac{\left| \frac{\Delta f_i}{\Delta \xi_j} \right|}{\sum_j \left| \frac{\Delta f_i}{\Delta \xi_j} \right|} \times 100\% \tag{2}$$

Second, take the bottom thickness S and undercut amount D as the system response, and select die depth h, rivet diameter d, rivet length L, die bottom radius r, die radius R, and punching speed v as the study variables for sensitivity analysis. Third, increase the six research variables by 10% in turn according to the principle of changing a single variable, conducting finite element simulation,

measuring the bottom thickness and undercut amount, and then comparing the prototype structure to obtain the bottom thickness and undercut amount increment. Table 5 shows specific value changes.

Table 5

Change of joint cross-section size caused by increment of research variable (mm)

	R	*r*	*h*	*v*	*d*	*L*
Original bottom thickness	2.1	2.1	2.1	2.1	2.1	2.1
Original bottom thickness after the increment	2.8	1.9	1.7	2.5	1.8	2.6
Increment of bottom thickness	0.7	-0.2	-0.4	0.4	-0.3	0.5
Original undercut amount	2.0	2.0	2.0	2.0	2.0	2.0
Original undercut amount after the increment	2.6	1.6	1.5	1.7	2.4	2.8
Increment of undercut amount	0.6	-0.4	-0.5	-0.3	0.4	0.8

According to the data in Table 5, use Equation (1) to calculate the sensitivity of each of the study variables. Finally, according to Equation (2), normalize the sensitivity to obtain the relative sensitivity of the bottom thickness and undercut amount. For example, the rivet length of the prototype structure is 6mm. After a 10% increase, the rivet length is 6.6mm. In ANSYS, only change the rivet length, and the other parameters remain unchanged. After carrying out finite element simulation, select the structure whose change of the bottom thickness is 0.5mm and the relative increment of the rivet parameters is 0.1. Use Equation (1) to calculate the sensitivity value is 5. After normalization, the relative sensitivity of the bottom thickness is 20%.

Considering the influence of the riveted joint parameters on the bottom thickness and undercut amount, use the average value of the impact of the dimensional variables on the bottom thickness and undercut amount as a comprehensive measure of the sensitivity of the dynamic structural performance to the dimensional structural parameters. Table 6 shows the relative sensitivity and integrated sensitivity values.

Table 6

dynamic performance sensitivity

Dimensional variables	Sensitivity analysis of the bottom thickness	Sensitivity analysis of undercut amount	Comprehensive sensitivity analysis
d	12.00%	13.33%	12.67%
L	20.00%	26.67%	23.34%
R	28.00%	20.00%	24.00%
r	8.00%	13.33%	10.67%
h	16.00%	16.67%	16.34%
v	16.00%	10.00%	13.00%

In summary, among the many parameters that affect the quality of a riveted joint, die radius R, rivet length L, and die depth h significantly impact the bottom thickness and the undercut amount of the riveted joints.

3.2 Analysis of the influence of riveting process parameters

According to the production parameters provided by the enterprise, control die radius, rivet length or die depth by a single variable and use finite element simulation to obtain the variation curves of the bottom thickness and the undercut amount under different structural parameters. Fig. 5 shows the specific variation curves.

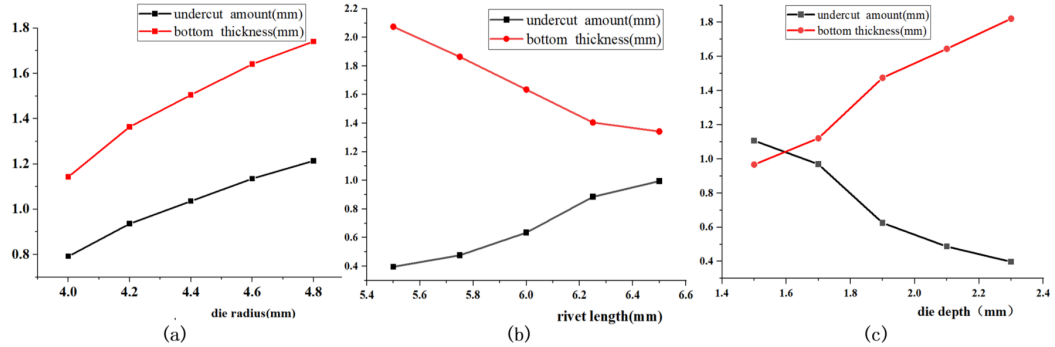

Fig 5 Self-thrust riveting simulation process.

When the rivet length and die depth are constant and the die radius is increased, the rivet foot is less constrained, the foot metal mobility is enhanced, and the foot opening angle is increased, resulting in an increase in bottom thickness and an increase in bottom cut, the values of which change as shown in Figure 5 (a). It is observed from the figure that the sensitive variation trend of the bottom thickness and the undercut amount is consistent. In the range of 4.2mm-4.8mm, the slope of both is less than that in the range of 4.00mm-4.2mm, and the slope in the range of 4.2mm-4.4mm is more pronounced than that in the range of 4.4mm-4.8mm, and the effect on the bottom thickness and dark cut volume decreases when the die radius exceeds 4.4mm. Therefore, the optimal structural parameters of the mold radius range are 4.0mm-4.4mm. Similarly, Figure 5 (b) analysis the impact of rivet length on joint performance and the effect of die depth on joint performance in Fig. 5 (c), obtaining the optimal structural parameters of the rivet length 6.0mm-6.5mm and die depth is 1.7mm-2.1mm.

4. Multi-objective model building and solving

4.1 Response surface modeling and analysis

In this study, we used central composite design experiments [15] to fit a response surface model of the riveted structural parameters. Develop a response surface model targeting bottom thickness S and undercut amount D using die radius R, rivet length L and die depth h as the influencing parameters. The parameters obtained in the previous section were entered into the response equation model, and the parameters for the 18 sets of central composite design

experiments were set using Design-expert software. The parameters of the experimental design section are shown in Table 7, and each set of data was calculated in ANSYS Workbench.

Table 7

Central composite design experiments table(mm).

Serial number	*R*	*L*	*h*	*S*	*D*	Serial number	*R*	*L*	*h*	*S*	*D*
1	4.40	6.50	2.10	1.138	0.548	10	4.20	6.25	1.90	1.172	0.613
2	3.86	6.25	1.90	0.682	0.624	11	4.20	6.25	1.90	1.172	0.613
3	4.20	6.25	2.24	1.268	0.476	12	4.2	5.83	1.90	1.674	0.572
4	4.40	6.00	2.10	1.402	0.425	13	4.20	6.25	1.90	1.172	0.613
5	4.20	6.25	1.90	1.172	0.613	14	4.40	6.50	1.70	0.837	0.641
6	4.40	6.00	1.7	1.425	0.797	15	4.00	6.00	2.10	1.485	0.742
7	4.20	6.25	1.90	1.172	0.613	16	4.00	6.50	2.10	1.165	0.824
8	4.20	6.25	1.56	1.024	0.825	17	4.00	6.50	1.70	0.974	0.914
9	4.20	6.67	1.90	0.723	0.804	18	4.54	6.25	1.90	1.276	0.867

As shown in Equation 3, to obtain the mapping relationships, fit a second-response surface linear equation to the variables in Table 7 using Design-expert to get the mapping relationships between the bottom thickness S and the independent variables die radius R, rivet length L, and die depth h.

$$S = 1.17 + 0.063R - 0.229L + 0.076h - 0.023RL - 0.009Rh + 0.044Lh - 0.49R^2 - 0.034L^2 - 0.014h^2 \quad (3)$$

Fig. 6 shows the relationship between the main research variables (Rivet length, Die radius and Die depth) and the bottom thickness according to Equation (3). It can more intuitively observe the impact of research variables on the bottom thickness.

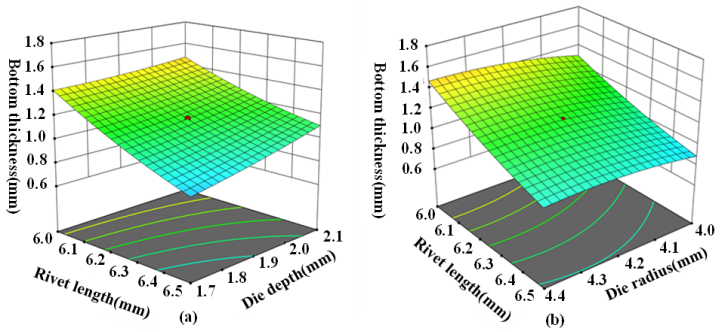

Fig 6 (a) The effect of rivet length and die depth on bottom thickness (b) The effect of rivet length and die radius on bottom thickness.

From the two-dimensional surface in Fig. 6 (a), it can be seen that the bottom thickness tends to increase with the increase of the die depth; with the increase of rivet length, the thickness bottom has a more obvious decreasing trend. It can be seen from the contour line at the bottom of Figure 6 (a) that when the die depth increases, the rivet length decreases, which can effectively increase the bottom thickness. From the two-dimensional surface in Fig. 6 (b), it can be seen

that with the increase of the die radius, the changing trend of the thickness bottom first increases and then decreases, reaching the maximum at about 4.24mm. It can be seen from the contour line at the bottom of Figure 6 (b) that when the die radius increases, the rivet length decreases, which can effectively increase the bottom thickness.

Similarly, the mapping relationship between the undercut amount and the independent variable is obtained in Equation 4.

$$D = 0.613 - 0.033R + 0.04L - 0.087h - 0.03RL - 0.04Rh + 0.03Lh - 0.048R^2 - 0.029L^2 - 0.015h^2 \quad (4)$$

Figure 7 shows the relationship between the main research variables (Rivet length, Die radius and Die depth) and the undercut amount according to Equation (4). It can more intuitively observe the impact of research variables on the undercut amount.

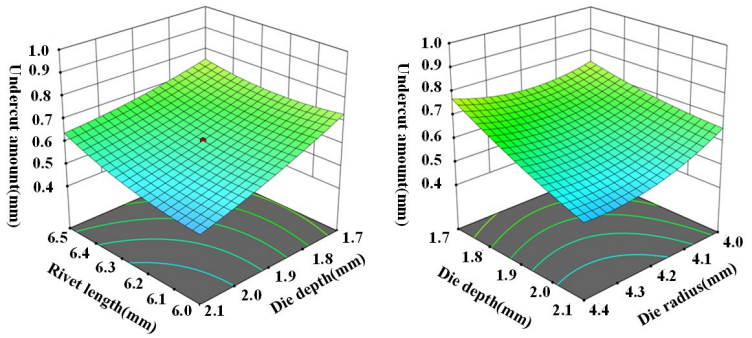

Fig 7 (a) The effect of rivet length and die depth on the length of undercut amount (b) Effect of die depth and die radius on the length of undercut amount.

From the two-dimensional surface of Figure 7 (a), it can be seen that the undercut amount tends to increase with the increase of rivet length; with the increase of die depth, the undercut has a more obvious downward trend. It can be seen from the contour line at the bottom of Figure 7 (a) that, while the rivet length is far away from 6.2mm, the reduction of die depth can effectively increase the undercut amount. From the two-dimensional surface in Fig. 7 (b), it can be seen that with the increase of the die radius, the changing trend of the undercut amount decreases first and then increases, reaching the minimum at about 4.2 mm. It can be seen from the contour line at the bottom of Figure 7 (b) that when the die radius is far away from 4.2mm, the reduction of die depth can effectively increase the undercut amount.

4.2 Self-punch riveting multi-objective optimisation

Take the bottom thickness and the undercut amount as the system response, and transform the standard form of the multi-objective optimisation model is transformed into the maximum solution form. Obtain the expression (5)

of the objective optimisation and the constraint expressions (6) of the multi-objective optimisation model.

$$\max\begin{cases} f_1 = \dfrac{S}{S_0} \\ f_2 = \dfrac{D}{D_0} \end{cases} \tag{5}$$

$$s.t.\begin{cases} 4.00mm \le R \le 4.40mm \\ 6.00mm \le L \le 6.50mm \\ 1.7mm \le h \le 2.1mm \\ f_i \ge 1 (i = 1,2) \end{cases} \tag{6}$$

In equation (5), S_0 denotes the bottom thickness before optimisation; and D_0 denotes the undercut amount before optimisation.

As the nature of genetic algorithms [16] is stochastic search, which cannot guarantee the resulting solution is optimal, especially in dealing with multi-peaked problems with multiple optimal solutions easily fall into local minima and stop searching, causing premature issues failing to achieve global optimality. Therefore, this paper uses the NSGA-II algorithm [17] to solve multi-objective optimisation models, modifying the non-dominated ranking genetic algorithm and reducing the computation's complexity. The introduction of an operation strategy expands the sampling space and improves the accuracy of the optimisation results. And also introduce the crowding degree and crowding comparison operator, ensuring the diversity of optimal solutions.

Use the NSGA-II multi-objective algorithm in the Isight software to optimise the bottom thickness and undercut amount parameters. Obtaining the Pareto solution with the objective of maximising bottom thickness and undercut amount. As shown in Figure 8, we can observe the distribution of the Pareto solution values in the plot through the Design Gateway window.

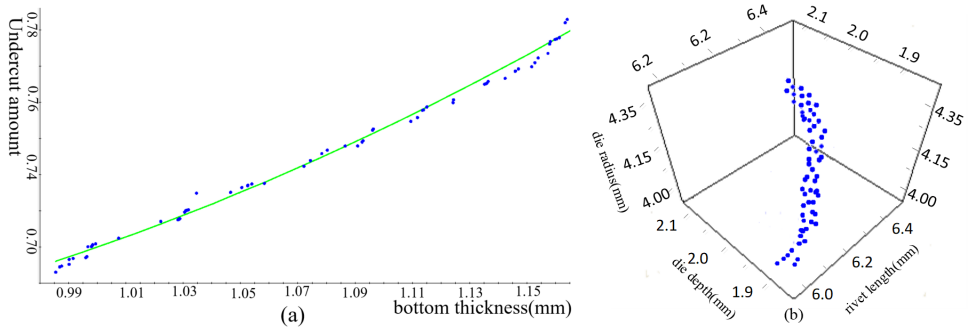

Fig 8 (a) Optimal solution distribution of undercut amount and bottom thickness. (b) The optimal solution of die depth, rivet length and die radius is distributed in a 3D view.

By analysing the distribution of the Pareto optimised solution set in 2D and 3D coordinates, combine the conclusions obtained in the previous section.

Recommend a set of the optimal solution in the setting of all solutions by Isight software, such as a die radius of 4.398mm, a rivet length of 6.496mm and a die depth of 1.986mm.

5. Test verification

5.1 Riveted joint cross-section measurement experiment

For the forming experiment of riveted joints, as shown in Fig. 9 (a), we use the JM20T-J-PLC precision hydraulic riveting machine provided by the company to the prototype sample of the high-speed rail top plates. As shown in Fig. 9 (b), we use a two-dimensional digital image measuring to measure the bottom thickness and undercut the amount of the riveted joint cross-section.

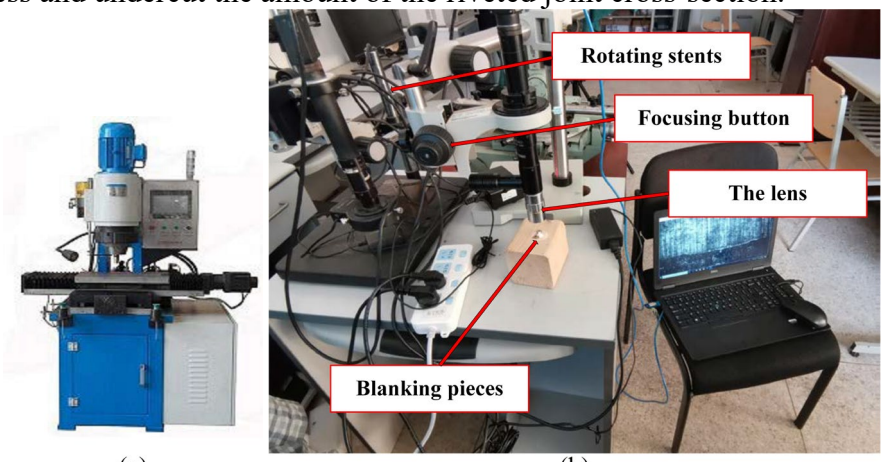

(a) (b)

Fig 9 (a) Precision riveting press (b) two-dimensional digital image measuring instrument.

In order to reduce the influence of random factors, perform 10 riveting joints before and after optimization, and then cut apart the joints using a cutter to measure the bottom thickness and undercut with the help of a measuring instrument. Fig. 10 shows one set of cross-sectional comparisons before and after optimization.

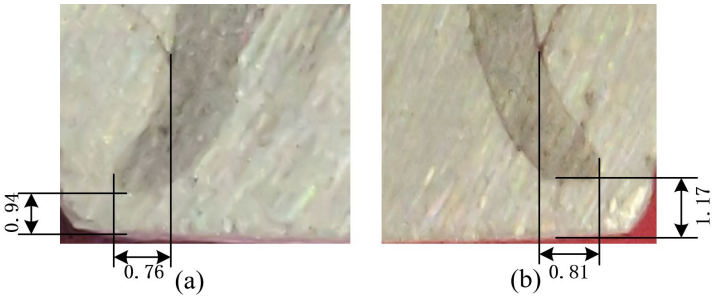

Fig 10 Cross-sectional comparison before and after optimisation

The measurements reveal that the bottom thickness and undercut amount of the optimised riveted joints met the constraints. Count the mean values of the cross-sectional parameters of the 10 riveted joints and compare them with those before optimization, as shown in Table 8.

Table 8

A comparison of the cross-sectional parameters

	Bottom thickness	Undercut amount
Pre-optimisation parameters	0.94mm	0.76mm
Optimised parameters	1.17mm	0.87mm
Improvement rate	24.7%	14.5%

Table 8 shows that the residual thickness and undercut amount of the riveted joint have improved significantly.

5.2 Mechanical properties of riveted joints experiment

Riveting strength evaluation is the essential part of joint quality evaluation. Insufficient riveting strength of the vehicle body will lead to severe consequences, and it is also the primary safety problem of the vehicle body. Usually, manufacturers consider axial and radial shear tensile tests to judge whether the strength of body riveted joints meets the requirements [18]. This paper mainly studies the riveted joint of high-speed rail body top plates. The main failure form affecting the riveting strength here is the radial shear tension of the joint. Therefore, we designed the mechanical tests for riveted joints according to the standard GB/T228-2010 "Room temperature tensile test methods for metallic materials" [19]. The experimental materials are taken from the prototype sample of the high-speed rail top plates, and the physical specimen after riveting is shown in Fig. 11(a). The tensile test is carried out with DWD-300 electro-hydraulic servo universal testing machine in Fig. 11 (b).

(a) (b)

Fig 11 (a) Physical view of the specimen (b) Electro-hydraulic servo universal testing machine

The ten static tensile load-displacement curves obtained before and after parameter optimisation are shown in Figure 12.

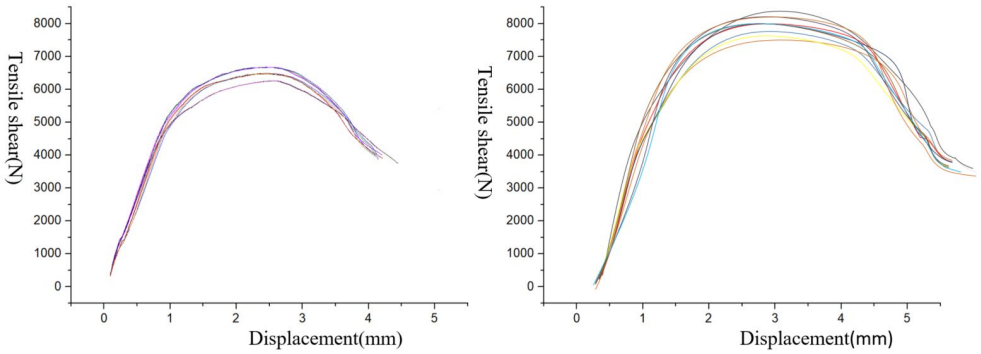

Fig 12 Riveting parameters optimize the static tensile load-displacement curve before and after

The results of the static tension experiments show that the maximum tensile shear force of the riveted parts before the optimization is 6.62 kN, the minimum tensile shear force is 6.02 kN, and the average tensile shear force is 6.26 kN. After optimization, the maximum tensile shear force of the riveted parts is 8.46 kN, the minimum tesile shear force is 7.51 kN, and the average tensile shear force is 7.98 kN. The average tensile shear force is increased by 27%. It can be seen from the experiments before and after optimization that the tensile performance of the optimised riveted parts has been significantly improved.

6. Conclusions

This paper uses sensitivity analysis to determine the main factors affecting the riveting process parameters and further determine their parameter ranges. Use central composite design experiments to establish a quadratic polynomial response surface model reflecting each parameter. Apply the NSGA-II algorithm to optimize the multi-objective model and arrive at the optimal combination of each parameter. Experiments show that the bottom thickness was improved by 24.7%, the undercut amount by 14.5%, and the tensile shear force by 27% compared to the performance of the joint before optimisation. This study has greatly improved the joint quality of the self-pierce riveted joints and is an essential guide for practical production.

Acknowledgement

The work is supported by the Shijiazhuang Guoxiang Transportation Equipment Company, Aluminum alloy self-piercing riveting simulation and experimental analysis.

REFERENCES

[1]. *Cai D G, Wei S W, Ye Y S, et al*. Mechanical properties of lightweight foam concrete filler for roadbed of high-speed railway[J]. Arabian Journal of Geosciences, 2021, 14(10): 1-10.
[2]. *Haque R.* Quality of self-piercing riveting (SPR) joints from cross-sectional perspective: A review[J]. Archives of civil and mechanical engineering, 2018, 18(1): 83-93.
[3]. *Carandente M, Dashwood R J, Masters I G, et al.* Improvements in numerical simulation of the SPR process using a thermo-mechanical finite element analysis[J]. Journal of Materials Processing Technology, 2016, 236: 148-161.
[4]. *Xie Y, Tan JJ, Cheng WW, et al.* Optimization of process parameters for semi-hollow self-punching riveting dies[J]. Automotive Technology and Materials, 2019, 8.
[5]. *Chung C S, Kim H K.* Fatigue strength of self-piercing riveted joints in lap-shear specimens of aluminium and steel sheets[J]. Fatigue & Fracture of Engineering Materials & Structures, 2016, 39(9): 1105-1114.
[6]. *Zhang Y H, Shi B J, Zhong J B.* Multi-parameter joint optimization of self-piercing riveting on aluminium alloy plate[C]//Journal of Physics: Conference Series. IOP Publishing, 2020, 1605(1): 012093.
[7]. Self-pierce riveting for perfect joints, Boellhoff cooperation, (2010).
[8]. *Zhao H, Han L, Liu Y, et al.* Modelling and interaction analysis of the self-pierce riveting process using regression analysis and FEA[J]. The International Journal of Advanced Manufacturing Technology, 2021, 113(1): 159-176.
[9] *A. Chrysanthou, X. Sun*, Self-piercing riveting: properties, Processes and Applications (2014).
[10] *J. Gårdstam*, Simulation and Verification of Strength of Self Pierced Rivet Joints of Stainless Sheet Steels, Swedish Institute for Metals Research, 2004 IM-2004-547.
[11]. *Hahn O, Kraus C, Leuschen G, et al*. Research in impulse joining of self pierce riveting[C]//3rd International Conference on High Speed Forming, March 11-12, 2008, Dortmund, Germany. Institut für Umformtechnik-Technische Universität Dortmund, 2008.
[12] Haque R, Beynon J H, Durandet Y. Characterisation of force–displacement curve in self-pierce riveting[J]. Science and Technology of Welding and joining, 2012, 17(6): 476-488.
[13]. *Ruijun L, Xiangwen D.* Weight analysis on parameters of self-pierce riveting[C]//2011 International Conference on Consumer Electronics, Communications and Networks (CECNet). IEEE, 2011: 1892-1895.
[14]. *Yin J, Gu J, Chen Y, et al.* Global sensitivity analysis of riveting parameters based on a random sampling-high dimensional model representation[J]. The International Journal of Advanced Manufacturing Technology, 2021, 113(1): 465-472.
[15]. *Jreissat M, Gharaibeh M A.* Analysis and optimization of the strain concentration factor in countersunk rivet holes via finite element and response surface methods[J]. Multidiscipline Modeling in Materials and Structures, 2020.
[16]. *Holland J H.* Genetic algorithms[J]. Scientific American, 1992, 267(1): 66-73.
[17]. *Deb K, Agrawal S, Pratap A, et al.* A fast elitist non-dominated sorting genetic algorithm for multi-objective optimization: NSGA-II[C]//International conference on parallel problem solving from nature. Springer, Berlin, Heidelberg, 2000: 849-858.
[18]. *Li Q, Xu C, Gao S, et al*. Study on the Influence Law of Forming Quality of Clinched Joint for Dissimilar Metal Sheet[J]. 2021.
[19]. GB/T228-2010/ISO 6892 Tensile test method for the metal materials at room temperature Standardization Administration of the People's Republic of China, 2010 (2009)